

# THE EFFECT OF COATING PROCESS THERMAL CYCLE ON MECHANICAL PROPERTIES OF AA6061-T6 USED FOR LOAD-CARRYING ELEMENTS OF A SPACE INSTRUMENT: A CASE STUDY

Tomasz Barciński<sup>1,\*</sup>, Robert Kosturek<sup>2</sup>, Tomasz Kowalski<sup>1</sup>, Maciej Bzowski<sup>1</sup>, Roman Wawrzaszek<sup>1</sup>, Karol Mostowy<sup>1</sup>, Jędrzej Baran<sup>1</sup>, Maciej Daukso<sup>1</sup>

<sup>1</sup> Space Research Center, Polish Academy of Sciences (CBK PAN), Warsaw, Poland

<sup>2</sup> Department of Fatigue and Machine Design, Faculty of Mechanical Engineering, Military University of Technology, Warsaw, Poland

**Abstract.** Components used for the structure of the GLOBal Solar Wind Structure experiment in the NASA Interstellar Mapping and Acceleration Probe space mission, made of AA6061-T6 alloy, are subjected to the coating process, where the temperature affects its mechanical properties. The aim of this paper is to examine the impact of the coating thermal cycle on the mechanical properties of AA6061-T6 alloy, which is the load-carrying material in a spaceborne instrument. As a part of the manufacturing process, the parts made of AA6061-T6 are subjected to a coating process at a temperature of about 220°C for a time longer than 1h. This treatment modifies the mechanical properties of the alloy. To evaluate the consequences of this change for spaceborne components, mechanical testing and numerical simulation were carried out. It was found that as a result of the coating process, the reduction in AA6061-T6 yield strength is about 16%, which entails a decrease in the margins of safety by 25% at its maximum.

**Keywords:** mechanical properties, aluminum, satellite, thermal cycle, safety factor

## 1. INTRODUCTION

The structure elements of scientific instruments for space applications are often made of aluminum alloys due to their good mechanical properties and low density [1-2]. The example of the aluminum-based space probe component which uses aluminum alloy AA6061-T6 as a construction material is the structure of the GLOBal Solar Wind Structure (GLOWS) experiment in the NASA Interstellar Mapping and Acceleration Probe (IMAP) space mission (Fig. 1).

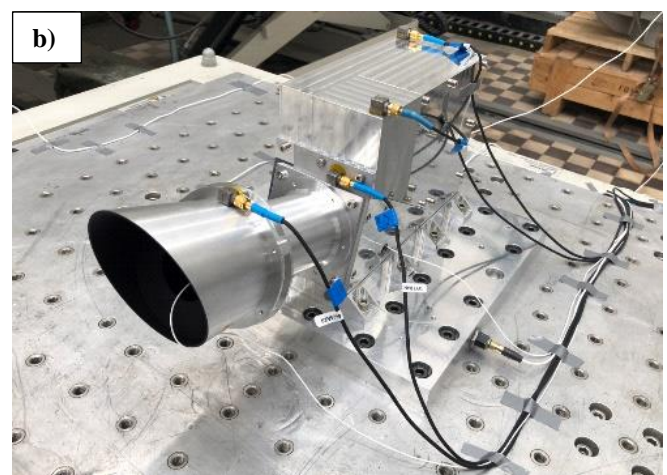
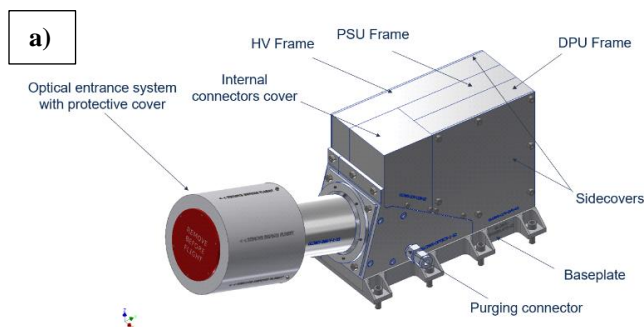


**Fig. 1.** GLOWS Design Model view (a), physical model during vibration testing (b). The abbreviations used are: PSU – Power Supply Unit, HV – High Voltage, DPU – digital Processing Unit. The approximate dimensions of the instrument are a cuboid with edges of 20x20x40 cm.

The mission is scheduled for launch into a Lissajous orbit around the Lagrange point L1 in 2026 [3]. The objective of

\*e-mail: tbarcinski@cbk.waw.pl

GLOWS is to investigate the global heliolatitude structure of the solar wind and its evolution during the solar cycle. Additionally, GLOWS investigates the distribution of interstellar neutral hydrogen (ISN H) and the solar radiation pressure acting on ISN H. The GLOWS detector is a non-imaging single-pixel Lyman- $\alpha$  photometer, effectively a photon counting instrument. It is conceptually based on the TWINS/LaD photometer originally designed to observe the terrestrial exospheric resonant Lyman- $\alpha$  glow [4-5]. The instrument includes a collimator with a baffle, a spectral filter, and a channeltron (CEM) detector. They are connected to the electronics block, responsible for collecting the event pulses and binning them for downlinking to the ground. The instrument is designed and assembled in the Space Research Centre, Polish Academy of Sciences (CBK PAN).

The instrument counts only photons entering it from a narrow cone with an opening angle of 4 degrees, therefore any straylight from reflections must be attenuated. For this, a baffle and a collimator covered with a material of appropriate optical parameters have been developed (Fig. 2).

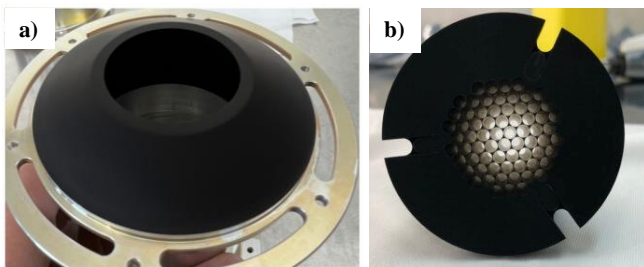


**Fig. 2.** Coated baffle element (a) and collimator (b) of the GLOWS instrument, shown as example.

Spaceborne instruments must be constructed sufficiently strong to survive without damage the inevitable launch stress. In most applications, the maximum loads on the spacecraft are during the launch. They are stochastic vibrations with almost all power contained in the bandwidth 20-2000 Hz, which are caused by the vibration of the rocket. Besides the vibrations, shock loads occur due to detachment of the rocket stages during the flight. In the instrument structure, the field of strength and strain caused by vibrations and shocks depends on the Young modulus, and it must not reach the yield strength with a specific safety margin of the material used.

As a part of the manufacturing process, some load-carrying elements of the instrument must be covered with thin layers of coatings to guarantee appropriate optical properties. The covering process involves heating to a temperature (e.g., 220°C) that exceeds the range of the maximum service temperature of the alloy (130°C) [6]. For the aluminum alloy AA6061-T6 used as the construction material, which is a precipitation-hardened alloy, its mechanical properties can be affected by the thermal cycle of the coating process. For the purpose of industrial applications, several studies have been carried out on this subject [7-10]. In the technical report on assessment of aluminum structural materials for service within the Advanced Neutron Source reflector vessel, the author stated that at temperature above 150°C, the AA6061-T6 alloy suffers

a loss in the strength, and the deterioration increases with time at temperature [7]. Polat et al. performed research on the effects of the artificial-aging on the mechanical properties of AA6061-T6 and reported a significant reduction in the hardness of the investigated alloy after passing the peak-aged state in 200°C [8]. The results overlap with the aging curves presented for the AA6061 alloy by Davis [9]. Generally, changes in the mechanical properties of AA6061 in the condition of a temperature above 150°C are hard to avoid due to the natural processes of overaging occurring in the alloy structure. During the precipitation hardening process, which consists of solution treatment and aging, the following transformations take place as a result of supersaturated solid solution (SSSS) decomposition: SSSS  $\rightarrow$  Si and Mg atomic clusters  $\rightarrow$  dissolution of Mg clusters  $\rightarrow$  Mg<sub>2</sub>Si co-clusters  $\rightarrow$  Guinier-Prestone-I zones  $\rightarrow$   $\beta''$  (GP-II zones) [8]. The  $\beta''$  is a coherent phase which hardens the alloy most effectively (peak aged). Nevertheless, it is a metastable phase and it further transforms:  $\beta'' \rightarrow \beta' \rightarrow \beta' \rightarrow \beta$  (Mg<sub>2</sub>Si, equilibrium phase). The natural consequence of these transformations (the so-called “overaging process”) are losses in the coherency between the crystal lattice of the alloy and the precipitates:  $\beta'$  and  $\beta'$  are semicoherent, and  $\beta$  is incoherent phase [10]. The microstructural changes affect the mechanical properties of AA6061. When  $\beta''$  transforms, the reduction in the tensile and yield strength is observed in favor of ductility [8,11]. Although the authors of these investigations agree that the drop in mechanical properties occurs, exact values have to be examined individually because they strongly depend on the temperature and time and can be estimated based on aging curves only approximately [8,9,11].

In the design of the GLOWS instrument, the most crucial mechanical properties taken into consideration are the yield strength and Young’s modulus. According to several studies, e.g., the research conducted by Summers et al., Young’s modulus of AA6061-T651 is nearly not affected by overaging [11]. At the same time, the temperature of 150°C begins to reduce the yield strength of the alloy, which, to a certain degree, can be estimated based on microhardness measurement [7,11,12]. Since the used alloy is in the peak-strength condition, and the approximate time of the exposure of the investigated component on the affecting temperature above 200°C is about 1.5h, some of the available literature data can be used for an estimation of the property change of the alloy. Jiang et al. investigated overaging of the AA6008-T4 alloy and reported that annealing in 215°C per 90 minutes results in an approximately 15% reduction in the microhardness value [13]. Additionally, they stated that also the yield strength was reduced (compared to the peak-strength condition) as a result of the  $\beta''$  phase transformation into  $\beta'$ . Referring to various studies focused on the prediction of the mechanical properties of the overaged AA6061 alloy it can be preliminarily estimated that the reduction of yield strength in the considered thermal cycle should be about 15% [11,14].

The instrument must safely sustain all the specified design loads without mechanical degradation. Factor of Safety (FoS) must account for inaccuracies in the predicted allowable values and applied stresses due to: analysis uncertainties, manufacturing

tolerances, scatter in the material properties. Safety factors are applied as multiplicative constants to the critical design loads to preclude material yield or failure at ultimate loads. The structure must demonstrate positive Margins of Safety for every element under all types of limitations, failure modes, and conditions associated with the loads specified. The following safety factor were considered:  $FoS = 1.6$  for the yield loads,  $FoS = 1.8$  for the ultimate loads. Lowering the yield or ultimate loads may lead to unacceptably narrow or even negative margins of safety.

## 2. EXPERIMENTAL

In order to evaluate the influence of the thermal cycle of the coating process on the properties of AA6061-T6, the tensile tests and microhardness analysis have been carried out. The thermal cycle of the coating process is presented in table 1.

**TABLE 1.** The thermal cycle of the coating process

Operation	Temperature	Time
Heating	25°C to 220°C	1.5 h
Soaking	220°C	1 h
Cooling	220°C to 50°C	2 h

The samples for the microhardness analysis were cut, mounted into resin and subjected to the conventional metallographic preparation, including grinding and polishing. To obtain the microhardness distribution, a microhardness tester Struers DuraScan 70 was used with an applied load of 0.98 N. The microhardness testing was conducted in accordance with the ASTM E384 standard. The mechanical properties were established in two different types of tensile test: on mini-specimens and the standard one. The reason for this approach is discussed in the further part of this paper. The geometries of the mini-specimen and the conventional specimen are presented in Fig. 3.

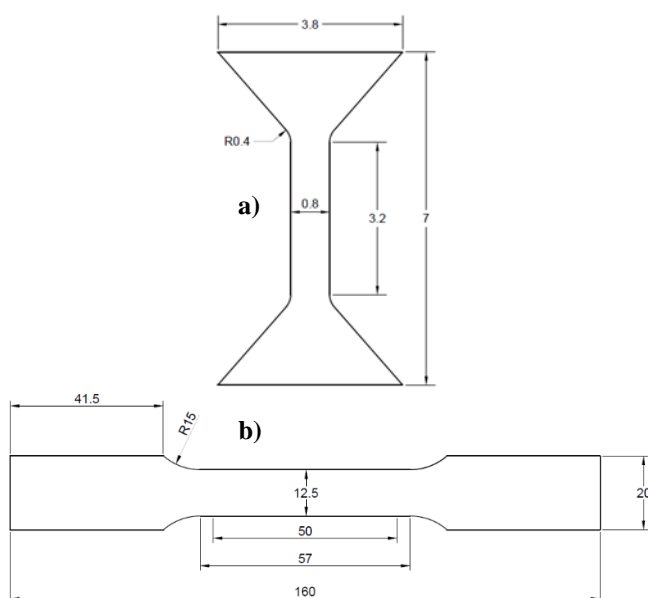


**Fig.3.** Schemes of the samples: mini-specimen (a), standard (b).

The tensile samples were cut using a CNC Accutex AL400 wire EDM machine. The samples in the as-received state and after the thermal cycles of the coating process were examined on Instron 8802 MTL supported by the WaveMatrix software in accordance with the ASTM E8/E8M standard.

Numerical modeling and simulations were performed in MSC Nastran with Patran pre- and postprocessing. The FEM model has been built using mainly QUAD4, HEX8 and CBAR elements. The model has been correlated with laboratory experiments, where accelerations on particular points of the instrument were measured and compared with the model predictions. The excitation put on the instrument in the boundary of its base was the stochastic acceleration with a bandwidth of 20 Hz – 2000 Hz.

## 3. RESULTS AND DISCUSSION

### 3.1. Initial research

For initial estimation of the influence of the coating process on the mechanical properties of AA6061 alloy, mini-specimens were tested. The reason for operating on mini-specimen was the fact that, initially, the only available piece of material after the coating process was the collimator. The collimator is composed of modules (slices) (Fig. 4) with a height allowing for coating the inside of the light tubes. Because in addition to the coated items also a non-coated collimator unit made of the same batch of the material, there was a possibility to do a comparison of selected mechanical properties between the coating-treated and pure items.

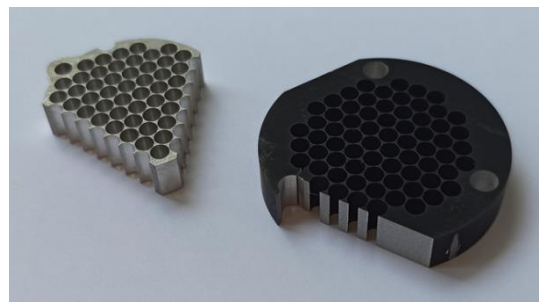


**Fig.4.** The collimator slices from which the mini-samples have been cut: the base material (left) and the material after the coating process (right).

The geometry of the mini-specimen, presented in Fig. 3a, was determined by the available amount of material to be examined. Although it did not allow to establish accurate material data (e.g. Young modulus, yield strength), it made possible only to compare the reported values of the ultimate tensile strength for the material in different states. In total, four samples of base material and three samples of coated material were examined. The obtained results are presented in Fig. 5.

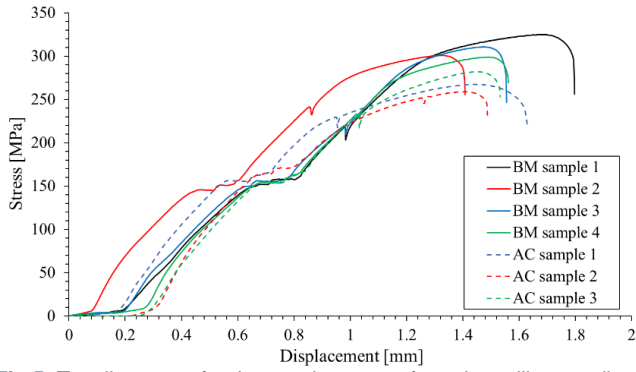


**Fig. 5.** Tensile curves for the specimens cut from the collimator slices: the base material (BM) and the material after coating process thermal cycle (AC).

The performed tensile tests show that the pieces of the AA6061-T6 alloy subjected to the coating process exhibit a noticeably lower tensile strength compared to the material in the as-received state. The calculated average value of the ultimate tensile strength for the base material is  $309.1 \pm 10.3$  MPa and for the coated material is  $269.6 \pm 9.5$  MPa. This result suggests an average reduction in the ultimate tensile strength by about 12.8%, but does not allow us to conclude on other parameters, e.g., yield strength. From the research conducted by Polat et al. a conclusion can be drawn that the decrease in the ultimate tensile and yield strength do not overlap, so an estimation is problematic to perform [5]. Also the obtained microhardness distribution gave information about the influence of the coating process thermal cycle on the material properties (Fig. 6).

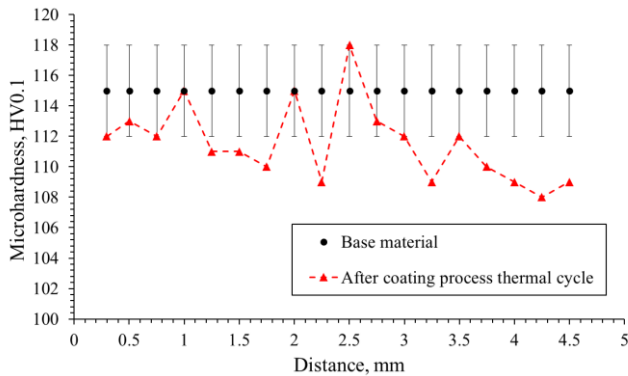


**Fig. 6.** Microhardness distributions in the element subjected to the coating process (the collimator) in relation to the values for the base material.

The obtained results indicate that the coating process thermal cycle reduced the microhardness value of the AA6061-T6 alloy. The average microhardness equals to  $115.0 \pm 1.9$  HV0.1 and  $111.5 \pm 2.6$  HV0.1 for the base and coated materials, respectively. The decrease in microhardness itself is not uniform and seems to concentrate at one of the outer surfaces of the tested fragment of the collimator (distances from 3.75 to 4.6 mm). Although the observed changes are relatively low, they slightly influence the susceptibility to plastic deformation of the component. Nevertheless, it is difficult to estimate the exact impact on the yield strength of the alloy because of the non-homogeneity and spread of the microhardness results.

### 3.2. Establishing mechanical properties after the coating process

The curves obtained in the tensile test for the base material (Fig. 7a) and the coated material (Fig. 7b) are presented below, and the established parameters are listed in Table 2.

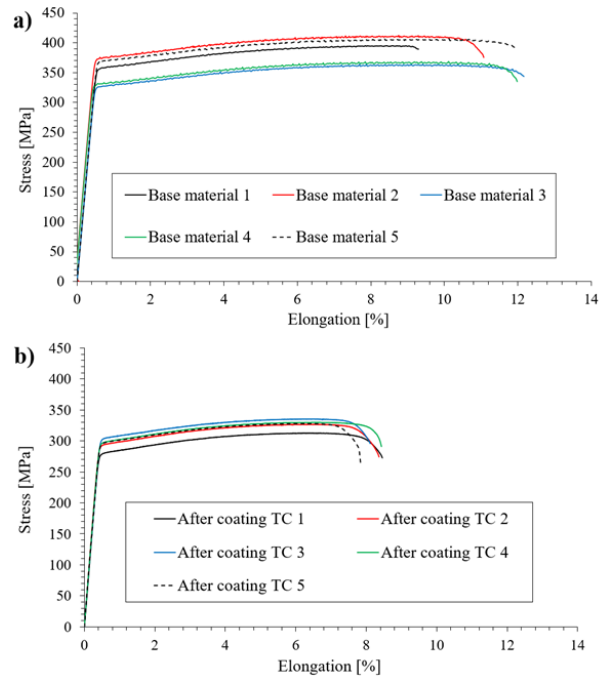


**Fig. 7.** Tensile curves obtained from: base material (a) and material after coating process thermal cycle (b).

**TABLE 2.** The established mechanical properties of the investigated samples

Description	Young modulus, E	Yield strength, R <sub>0.2</sub>	Ultimate tensile strength, R <sub>m</sub>	Elongation at break, A
Base material	$69.4 \pm 0.8$ GPa	$351.6 \pm 17.8$ MPa	$389.2 \pm 18.0$ MPa	$11.3 \pm 1\%$
After coating	$70.9 \pm 1.1$ GPa	$295.6 \pm 7.1$ MPa	$326.5 \pm 7.5$ MPa	$8.2 \pm 0.2\%$
Average change	1.5 GPa	-56.0 MPa	-62.7 MPa	-3.1 %

The obtained results indicate a significant effect of the temperature (220°C) accompanying the coating process on the strength properties of the AA6061-T651 alloy, especially the yield strength and tensile strength. The values of both of these strength parameters decreased by approx. 16%, corresponding to 56 MPa for the yield strength and 63 MPa for the tensile strength, respectively. In terms of yield strength, the established decrease (16%) mostly coincides with the preliminary value estimated in Section 1 (15%). At the same time, a deterioration of the ductility of the tested alloy was found, manifested by a lower value of elongation to break. The most serious consequence for the considered component is the decrease in the value of the yield strength, for it influences its safety factor. Relating the obtained results to the

current state of the art, a high level of convergence can be observed. The determination of the strength reduction in components during manufacturing and in service, including aluminum elements, has been the subject of numerous studies [15-20]. The participation of strengthening phase in AA6061 alloy significantly influences its strength parameters, with the highest yield strength and tensile strength values achieved in the T6 temper state [17-19]. Referring to investigations performed by P. T. Summer et al. and by M. Song, it was estimated that the applied thermal cycle will decrease the yield strength of the analyzed alloy by about 15%, which does not deviate significantly from the obtained value. [11,14]. Considering the determined values and standard deviations of the Young's modulus, they do not conclusively indicate whether the thermal cycle of the coating process had any influence on this parameter (tab. 2). This indirectly corresponds to the findings of Summers et al., suggesting that the overaging process of a similar alloy, AA6061-T651, does not affect its Young's modulus [11]. Overall, the obtained results are a typical effect of overaging of the strengthening phase. However, the precise determination of the strength parameters of the examined alloy after the coating process lays the groundwork for evaluating the safety of the constructed space instrument components.

### 3.3. Consequences for the instrument component

FEM simulations were performed in the NASTRAN environment. All structural elements were simulated mainly using QUAD4, HEX8 and CBAR elements. The FEM model used elastic models in which plastic deformation does not occur. This simplification is possible because the simulations used loads equal to the expected loads during space flight, in which the obtained loads were in the elastic range. The designed structure had been numerically tested in terms of von Mises stress field by Finite Elements Method (FEM). For this, numerical simulation of the launch were performed (Fig. 8). The random vibration loads were put on each axis of the instrument separately, and von Mises stresses computed. Results of analysis of the obtained margins of safety (MoS) and factors of safety (FoS) in terms of different values of yield strength (YS) and ultimate tensile strength (UTS) is presented in Table 3.

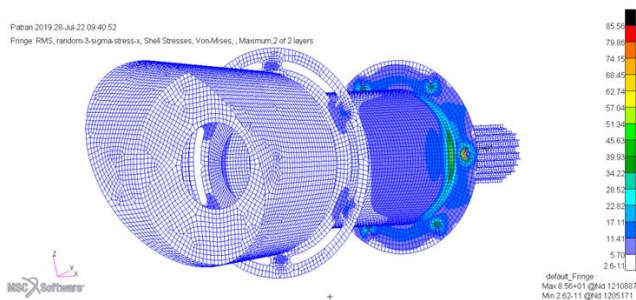


**Fig.8.** FEM numerical simulation of stress field on the instrument optical part. The approximate dimensions are a cylinder 10 cm in diameter and the height of 25 cm.

**TABLE 3.** Stresses and margins of safety for random vibration response

Load	X axis		Y axis		Z axis	
	BM	AC	BM	AC	BM	AC
YS [MPa]	333.8	288.5	333.8	288.5	333.8	288.5
UTS [MPa]	371.2	319	371.2	319	371.2	319
von Mises stress [MPa]	99.09					
FoSY	1.6					
FoSU	1.8					
MoSY	1.10	0.82	3.95	3.28	2.41	1.95
MoSU	0.87	0.79	3.40	3.21	2.03	1.90
MoSY % change	-	-25%	-	-17%	-	-19%
MoSU % change	-	-9%	-	-6%	-	-17%

The coating process has significantly changed the margins of safety, by lowering them. The strongest reduction was found in the axis X for the yield strength (-25%). Nevertheless, the margins remained positive. In the considered case, the initial margins were wide (above 1), therefore the thermal cycle related to the coating process has not resulted in a need to modify the design. However, the modification of the strength caused by this coating process thermal cycle must be taken into consideration during designing stress-carrying parts subjected to thermal treatment.

## 4. CONCLUSIONS

The aim of the work was to analyze the impact of the blackening process on the mechanical strength of a scientific instrument for a space mission. Using numerical simulation of stresses and comparing the results of tensile strength tests, we formulate the following conclusions:

1. The discussed coating process thermal cycle influenced the mechanical properties of AA6061-T6 alloy, reducing both ultimate and yield stress by about 16%.
2. The reduction of mechanical properties has been partly evaluated based on mini-specimen testing as 13%, which was a slight underestimation.
3. Implementation of a coating process for the load-carrying aluminum components that involves heating has consequences for the margins of safety. In the most severe load case, the margins are reduced by about 25%. While this is an acceptable value for the GLOWS instrument, potential reduction of safety margins in the mechanical design due to thermal treatment of load-carrying elements needs to be carefully considered, even in seemingly safe cases of treatment only comprising a surface coating.

## ACKNOWLEDGEMENTS

This research was supported by the GLOWS project under contract with Polish Ministry for Education and Science MEiN/2021/21/DIR/

## REFERENCES

- [1] A. M. A. El-Hameed and Y. A. Abdel-Aziz, "Aluminium Alloys in Space Applications: A Short Report," *Journal of Advanced Research in Applied Sciences and Engineering Technology*, vol. 22, no. 1, Art. no. 1, Jan. 2021, doi: 10.37934/araset.22.1.17.
- [2] S. V. S. Narayana Murty and S. C. Sharma, "Materials for Indian Space Program: An Overview," *J Indian Inst Sci*, vol. 102, no. 1, pp. 513–559, Jan. 2022, doi: 10.1007/s41745-021-00284-8.
- [3] D. J. McComas et al., "Interstellar Mapping and Acceleration Probe (IMAP): A New NASA Mission," *Space Sci Rev*, vol. 214, no. 8, p. 116, Oct. 2018, doi: 10.1007/s11214-018-0550-1.
- [4] H. U. Nass, J. H. Zoenchen, G. Lay, and H.-J. Fahr, "The TWINS-LAD mission: Observations of terrestrial Lyman- $\alpha$  fluxes," *Astrophysics and Space Sciences Transactions*, vol. 2, pp. 27–31, Jan. 2006, doi: 10.5194/astra-2-27-2006.
- [5] D. J. McComas et al., "The Two Wide-angle Imaging Neutral-atom Spectrometers (TWINS) NASA Mission-of-Opportunity," *Space Sci Rev*, vol. 142, no. 1, pp. 157–231, Feb. 2009, doi: 10.1007/s11214-008-9467-4.
- [6] K. Farrell, "Materials Selection for the HFIR Cold Neutron Source; TOPICAL," United States, Aug. 2001.
- [7] K. Farrell, "Assessment of aluminum structural materials for service within the ANS reflector vessel," United States, 1995.
- [8] A. Polat, M. Avsar, and F. Ozturk, "Effects of the artificial-aging temperature and time on the mechanical properties and springback behavior of AA6061," *Materiali in Tehnologije*, vol. 49, pp. 487–493, Aug. 2015, doi: 10.17222/mit.2013.154.
- [9] J. R. Davis, *Aluminum and Aluminum Alloys*. ASM International, 1993.
- [10] P. Dumitraschkewitz, S. S. A. Gerstl, L. T. Stephenson, P. J. Uggowitzer, and S. Pogatscher, "Clustering in Age-Hardenable Aluminum Alloys," *Advanced Engineering Materials*, vol. 20, no. 10, p. 1800255, 2018, doi: 10.1002/adem.201800255.
- [11] P. T. Summers et al., "Overview of aluminum alloy mechanical properties during and after fires," *Fire Science Reviews*, vol. 4, no. 1, p. 3, Apr. 2015, doi: 10.1186/s40038-015-0007-5.
- [12] F. Ozturk, A. Sisman, S. Toros, S. Kilic, and R. C. Picu, "Influence of aging treatment on mechanical properties of 6061 aluminum alloy," *Materials & Design*, vol. 31, no. 2, pp. 972–975, Feb. 2010, doi: 10.1016/j.matdes.2009.08.017.
- [13] G. D. Jiang, Y. H. Cai, C. Qiu, W. W. Zhang, and D. T. Zhang, "Effect of over-aging on the microstructure, mechanical properties and crashing performance of thin-walled Al–Mg–Si–Cu alloy profiles," *Journal of Materials Research and Technology*, vol. 21, pp. 3074–3085, Nov. 2022, doi: 10.1016/j.jmrt.2022.10.137.
- [14] M. Song, "Modeling the hardness and yield strength evolutions of aluminum alloy with rod/needle-shaped precipitates," *Materials Science and Engineering: A*, vol. 443, no. 1, pp. 172–177, Jan. 2007, doi: 10.1016/j.msea.2006.08.025.
- [15] S. V. Panin, P. O. Maruschak, I. V. Vlasov, A. S. Syromyatnikova, A. M. Bolshakov, F. Berto, O. Prentkovskis, B. B. Ovechkin, "Effect of Operating Degradation in Arctic Conditions on Physical and Mechanical Properties of 09Mn2Si Pipeline Steel," *Procedia Engineering*, vol. 178, pp. 597–603, Jan. 2017, doi: 10.1016/j.proeng.2017.01.117.
- [16] A. V. Byakov, A. V. Eremin, R. T. Shah, M. V. Burkov, P. S. Lyubutin, S. V. Panin, P. O. Maruschak, A. Menou, L. Bencheikh, "Estimating mechanical state of AA2024 specimen under tension with the use of Lamb wave based ultrasonic technique," *Molecular Crystals and Liquid Crystals*, vol. 655, no. 1, pp. 94–102, Sep. 2017, doi: 10.1080/15421406.2017.1360700.
- [17] S. Hussein, M. Al-Shammari, A. Takhakh, and M. Al-Waily, "Effect of Heat Treatment on Mechanical and Vibration Properties for 6061 and 2024 Aluminum Alloys," *Journal of Mechanical Engineering Research and Developments*, vol. 43, pp. 48–66, Jan. 2020.
- [18] G. Wang, G. Zhu, T. Li, and L. Kou, "Effect of heat treatment conditions on mechanical properties and springback of 6061 Aluminum alloy sheets," *IOP Conference Series: Materials Science and Engineering*, vol. 788, p. 012056, Jun. 2020, doi: 10.1088/1757-899X/788/1/012056.
- [19] K. Kadhim Hameed, K. Musa, and H. Dawood, "Investigation of Microstructural and Mechanical Properties of AA6061 alloy after heat treatment effects," *Journal of Advanced Research in Dynamical and Control Systems*, vol. 10, pp. 1835–1839, Jan. 2018.
- [20] W. Liu, S. Huang, S. Du, T. Gao, Z. Zhang, X. Chen, L. Huang, "The Effects of Heat Treatment on Microstructure and Mechanical Properties of Selective Laser Melting 6061 Aluminum Alloy," *Micromachines*, vol. 13, no. 7, p. 1059, Jun. 2022, doi: 10.3390/mi13071059.